Journal of Power Sources 659 (2025) 238429

Contents lists available at ScienceDirect

Journal of Power Sources

journal homepage: www.elsevier.com/locate/jpowsour

Assessing the H_2S-induced resistance increase of a Ni/GDC cermet electrode under OCV and cathodic polarization

D. Esau [a,*], S.A. Horlick [b], C.-Y. Tsai [b], A. Weber [a]

[a] Institute for Applied Materials – Electrochemical Technologies (IAM-ET), Karlsruhe Institute of Technology (KIT), Adenauerring 20b, Karlsruhe, D-76131, Germany
[b] Sunfire SE, Gasanstaltstraße 2, D-01237, Dresden, Germany

HIGHLIGHTS

- H_2S poisoning of Ni/GDC electrodes under steam and CO_2 electrolysis conditions.
- Interrelations between poisoning response, concentration and current resolved.
- Tafel behavior explains mitigation of resistance increase in H_2O electrolysis.
- In CO_2 electrolysis, cathodic current was found to mitigate H_2S poisoning.

ABSTRACT

It is widely accepted that sulfur-induced resistance increase is mitigated by the anodic current density in the fuel cell mode. On the other hand, the role of cathodic current in the electrolyzer mode is yet only poorly explored. This study therefore aims to identify the role of cathodic current on the poisoning behavior in solid oxide electrolyzers. We have performed an electrochemical impedance spectroscopy-based study on a commercial Ni/GDC electrode in a H_2S concentration range from 0.1 ppm to 1 ppm and current densities from 0 Acm^{-2} up to -1 Acm^{-2} in steam-electrolysis and up to -0.8 Acm^{-2} in CO_2-electrolysis. Results at OCV show a critical influence of H_2 and CO concentration on the poisoning response. Under cathodic polarization, the impact of sulfur on the resistance is lower when load is applied, compared to the OCV case, and this effect is more pronounced during CO_2-electrolysis than in H_2O-electrolysis. In poisoned H_2O-electrolysis, the electrode overpotentials match expectations from the inherent Tafel behavior of the electrode. In contrast, overpotentials during poisoned CO_2-electrolysis appear to be lower than one would expect from the inherent Tafel behavior of the electrode, demonstrating a mitigation effect of cathodic current on the H_2S poisoning in CO_2-electrolysis.

1. Introduction

High temperature solid oxide electrolyzers (SOEs) are an attractive technology for energy storage and the production of green chemicals. They stand out due to their exceptionally high electrical efficiencies and their capability to also convert carbon dioxide (CO_2) for renewable syngas production [1,2]. However, trace contamination in the feed gas of an electrolyzer can have detrimental influence on performance and durability. Sulfur is a commonly found contaminant in feed gases for CO_2- or co-electrolyzers [3]. Sulfur species present in the feed gases may include oxidized (SO_x) and reduced sulfur species (H_2S and COS) [4]. However, at elevated temperatures and under reducing conditions, sulfur species are most stable in their reduced form [5,6]; and, in the presence of a metal catalyst, oxidized species can be expected to reduce quickly to H_2S or COS.

In the form of H_2S, sulfur is known to harm the electrochemical performance of a cermet electrode via reversible adsorption on metal sites and subsequent blocking of active electrochemical sites:

$$H_2S \rightleftharpoons H_2 + S_{(ads)} \quad [1]$$

Earlier research has shown that the coverage of nickel with sulfur (Θ_S) can be expressed as a function of temperature T, p_{H_2} and p_{H_2S} [7]:

$$\Theta_S = 1.45 - 9.53 \cdot 10^{-5} T + 4.17 \cdot 10^{-5} T \ln\left(\frac{p_{H_2S}}{p_{H_2}}\right) \quad [2]$$

This isotherm was later used in Ref. [8] to show that the relative resistance increase, as well as the relative performance loss in hydrogen fuel cell operation, can be correlated linearly to the degree of coverage.

Similar correlations can be expected under a carbonaceous atmosphere. Riegraf et al. calculated that COS would be the most stable sulfur compound in a gas atmosphere consisting of CO and CO_2 at 860 °C [3]. However, the interaction between carbonyl sulfides and nickel surfaces is poorly explored and an isotherm that describes their adsorption

* Corresponding author.
E-mail address: daniel.esau@kit.edu (D. Esau).

https://doi.org/10.1016/j.jpowsour.2025.238429
Received 21 July 2025; Received in revised form 3 September 2025; Accepted 16 September 2025
Available online 23 September 2025

equilibrium is currently not available. Yet, it follows that operation conditions can significantly affect the poisoning response due to H_2S. Many studies have experimentally analyzed effects of temperature, feed gas composition and H_2S-concentration [9–13], basically confirming the negative effects of:

- low T,
- decreasing p_{H_2},
- increasing p_{H_2S} with a saturation effect towards higher concentrations.

These findings seem to be valid under open circuit voltage (OCV) as well as under polarization. Interestingly, multiple authors observed that the (relative) resistance increase due to H_2S is lower with current load in fuel cell mode, compared to the OCV case [8,9,12,14]. Other groups have only partly observed this effect [13], or not at all [15].

However, the reason for the often-observed mitigation effect has been under discussion and multiple mechanisms have been proposed. Most commonly, it is speculated that an increased flux of oxygen ions at the triple- (or double-) phase boundaries oxidizes adsorbed sulfur, so that the sulfur coverage is reduced [8,14,16]. A reversion of this effect could be theoretically expected in electrolysis mode. Contradictory to this idea, it was suggested that improved kinetics due to increasing steam contents at the electrochemically active region [12] or trivial anodic activation [17–19] can explain an apparently improved sulfur tolerance under anodic polarization.

Most of the earlier and present studies have focused mainly on the fuel cell mode, analyses of sulfur-induced performance losses in electrolysis mode are rare. Jeanmonod et al. have performed poisoning tests under co-electrolysis operation and have seen a lower impact of sulfur on the resistance compared to the OCV case. However, they could not exclude an influence of the previous testing history on the observed behavior [20]. Skafte et al. observed a significant harming effect of H_2S concentrations down to 20 ppb in CO_2-electrolysis with a Ni/YSZ fuel electrode [21].

Studies on the effect in steam electrolysis are currently not available, to the best of our knowledge. This might be due to the fact that sulfur contaminations in steam feeds can be expected to be low. However, such an investigation might be useful to better understand the poisoning behavior in co-electrolysis mode. Also, experiments under H_2/H_2O atmospheres can serve as a model system with highly-defined H_2S concentrations, compared to carbonaceous atmospheres where even 99.995 % pure gas supplies from commercial vendors might contain non-negligible traces of sulfur species [3,22].

Nickel/gadolinia-doped ceria (Ni/GDC) is a widely investigated alternative to the classical Ni/YSZ fuel electrode and has already reached commercialization through several companies [23–25]. Numerous studies have confirmed its high electrochemical activity for steam electrolysis, co-electrolysis, and CO_2 electrolysis [26–33]. While the use of Ni/GDC in CO_2 electrolysis can be limited by the susceptibility of nickel to catalyze the Boudouard reaction [21], its higher tolerance toward sulfur poisoning compared to Ni/YSZ [34,35] makes it particularly attractive for fundamental studies on sulfur poisoning behavior.

This study aims to improve the general understanding of the poisoning behavior under OCV and load, with a focus on cathodic polarization of the fuel electrode. We show how the partial pressure of steam and hydrogen influence the poisoning response. We try to correlate the results with the sulfur coverage of nickel, calculated from the Temkin isotherm presented in Ref. [7]. Further, we performed experiments under varying electrolysis load and quantified the relative resistance increase ($\Delta ASR_{Pol,rel}$) due to the H_2S-poisoning. It is demonstrated that the relative resistance increase is an unsuitable measure to investigate the influence of polarization. An alternative approach, based on comparing the theoretical and experimentally observed overpotential, is presented. Ultimately, the approach is transferred to CO_2-electrolysis, where increasing current was found to visibly mitigate the poisoning effect of H_2S.

2. Materials and methods

2.1. Cells and testbench specifications

Planar cells with an active area of 1 cm^2 were analyzed in this study. The cells were fabricated by *Sunfire SE* and exhibit a Ni/GDC fuel electrode and an LSCF air electrode on a 3 mol% yttria stabilized zirconia (3YSZ) electrolyte, which was supplied by *Kerafol GmbH & Co. KG* under the scope of the German H2Giga project (see acknowledgements). Standardized reduction procedures are always performed during the startup of every cell. Electrochemical measurements were performed with a two electrode setup in a test rig described in Ref. [36].

To generate well-defined H_2/H_2O-mixtures, synthetic steam was produced in an upstream combustion chamber by mixing appropriate amounts of oxygen with the fuel. CO/CO_2-mixtures were produced by mixing the two gases. H_2S, diluted in nitrogen, was added to the gas mixtures. For $H_2O/H_2/N_2$ mixtures N_2 and H_2S were added downstream of the combustion chamber. To ensure comparability, the total N_2+H_2S amount was kept constant during H_2S variations. Considering the bottled H_2S/N_2 gas mixture containing 0.01 % H_2S a minimum N_2+H_2S concentration of 5 % was required to achieve a reasonable waiting time for the onset of the poisoning response. The H_2S concentration is controlled by adjusting the H_2S/N_2-ratio, so that a total flow rate of 200 sccm was kept constant. Compressed air was always used on the air side and was supplied at a rate of 200 sccm.

Impedance spectra were acquired by a Solartron 1260 frequency response analyzer using a pseudo-potentiostatic measurement technique [36]. To keep the stimulus in a linear range, a current amplitude resulting in a $\leq$ 12 mV voltage drop with respect to polarization resistance was selected. Every measurement was performed in a frequency range between 30 mHz and 1 MHz with 12 points per decade. Impedance data quality was checked by a Kramers-Kronig test [37]. Fitting of EIS data was performed with in-house software. The derived distribution of relaxation times (DRT) showed the presence of up to four peaks. Polarization resistances were obtained by fitting the whole spectra to four R-CPE-elements in series, as shown in Fig. 1. The model resulted in a sufficiently good fit for all analyzed spectra. Relative errors were always under 0.5 %.

The resistance value of the R-CPE-element with the highest characteristic frequency was not included in the final polarization resistance, as its fit-value was found to be sensitive to high-frequency measurement artefacts. Our previous study on symmetrical cells with microstructurally similar Ni/GDC electrodes showed that resistance contributions with characteristic frequencies above 1 kHz are not affected by sulfur poisoning [32]. In the present work, no correlation of high-frequency contributions with sulfur poisoning was observed either, as shown in Figure S1. This observation is consistent with previous studies on Ni/GDC symmetrical cells, which report that impedance contributions related to the coupling of surface reaction and ionic transport typically occur at frequencies below 200 Hz [32,33,38]. For a detailed list of loss contributions in the EIS of Ni/GDC electrodes, we refer to our earlier work [32]. Furthermore, earlier measurements on symmetrical GDC/LSCF air electrodes with the same microstructure revealed an air electrode contribution of ~20 mΩcm^2 in total, comprising a gas diffusion contribution at ~4 Hz and oxygen surface exchange and transport resistances appearing at frequencies around 200 Hz and higher [33].

2.2. Testing protocol

After heating up, sealing the cell above operating temperature, and reducing the cell in H_2, the performance was checked to ensure that initial characteristics were comparable to previous investigations with the same cell type. Then, cell #1 was operated in the SOEC mode at a

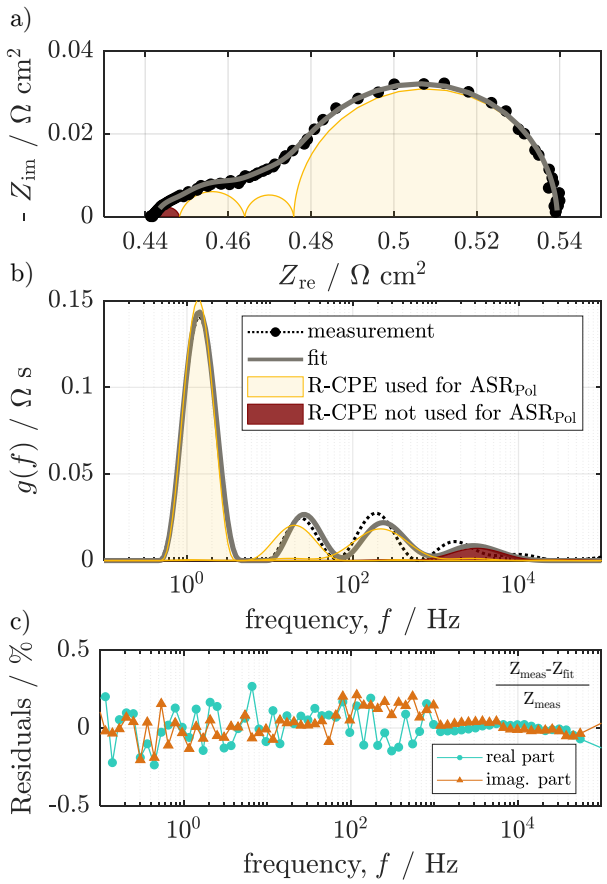

Fig. 1. **a)** Exemplary spectrum of the cell recorded with 0.92 atm H_2, 0.03 atm H_2O, balanced in nitrogen with no H_2S added. **b)** Derived DRT showing the presence of up to four main peaks. **c)** Real and imaginary fit residuals showing a relative error <0.5 %. The R-CPE element with the highest characteristic frequency was not included in the calculation of the polarization resistance as its fit value was sensitive towards high-frequency measurement artefacts. T = 860 °C, OCV.

current density of −0.6 Acm^{-2} (0.8 atm H_2O, bal. H_2, 800 °C) for 100 h. Afterwards the temperature was increased to 860 °C to record the poisoning behavior.

A protocol that involved the testing of various $H_2O/H_2/N_2$ ratios which were set under electrolysis and fuel cell loads in a range from −1 Acm^{-2} to 0.8 Acm^{-2} was developed and repeated in the following manner to obtain values for various H_2S concentrations:

1. Perform the protocol (current density and concentration variation) initially sulfur-free.
2. Add 0.1 ppm H_2S and observe ASR_{Pol} until sufficient stabilization.
3. Perform the protocol under 0.1 ppm H_2S.
4. Stop H_2S addition to check for regeneration.

Steps 2–4 were then repeated with 0.3 ppm, 0.5 ppm and 1 ppm. In order to confirm the actual concentration of H_2S and exclude the formation of other sulfur species in the gas phase, the thermodynamic equilibrium (including S_2, SO_2, SO_3, H_2S) was calculated with the software tool *Cantera* for every tested concentration in $H_2O/H_2/N_2$ mode. Results are displayed in the ESI in Table S1 and confirmed that the equilibrium concentration of H_2S was very close to the set concentration.

The current density range was chosen to cover a broad spectrum of operating modes close to actual stack conditions. The limits were defined to maintain a safe operating window between 0.6 V and 1.5 V, thereby ensuring sufficient distance from the nickel oxidation potential and the zirconia electrolyte reduction potential, respectively [36,39].

The data from cell #1 was used to generate Figs. 1–5. Recordings of resistance contributions of all performed EIS measurements, including stabilization and regeneration steps of cell #1, are given in the ESI in Figure S2.

The minimum time needed to cover all available Ni sites [40] with sulfur was calculated to be around 3 min, when assuming: 1) full coverage, 2) no interaction of the sulfur with upstream components, and 3) no transport limitations. In reality, the time to reach a stable polarization resistance after poisoning is in the range of several hours [41]. In our case stabilization periods ranged between 10 h (0–1 ppm @ 0.92 atm H_2, 0.03 atm H_2O, bal. N_2) and 250 h (0–0.1 ppm @ 0.15 atm H_2, 0.8 atm H_2O, bal. N_2). The vast differences in stabilization times might be related to transport limitations at low H_2S concentrations, or an influence of H_2 concentration on the adsorption rate. However, the focus of this publication is not related to the dynamic poisoning behavior, but rather an attempt to quantify the cell resistances at a close to stationary operating point.

To generate results under $CO_2/CO/N_2$ atmospheres (Figs. 6–8), a second cell was used (cell #2) and started up with the identical procedure as cell #1. A shorter protocol was employed with cell #2, which contained tests in a current density range from 0 Acm^{-2} to −1 Acm^{-2} at CO partial pressures of 0.15 atm, 0.1 atm and 0.05 atm (0.8 atm CO_2, bal. N_2, 860 °C). The protocol was repeated three times. The first set was performed without initial stabilization, where an increase in polarization resistance was observed over testing time. This increase might be attributed to trace sulfur contamination in the carbonaceous feed gas [3]. Indeed, traces of SO were confirmed via mass spectrometry to be present in the CO_2 gas supply.

After regenerating for 5 h in pure hydrogen, the cell was then left for 24 h in a 0.8 atm/0.15 atm/0.05 atm $CO_2/CO/N_2$ mixture under OCV. As the polarization resistance reached a stable point, a second dataset was recorded, which was then used as reference for calculating the respective $\Delta ASR_{Pol,rel}$. A final third dataset was then recorded after increasing the H_2S concentration by 1 ppm and subsequent stabilization. Again, thermodynamic calculations were performed to identify the most stable sulfur species in the gas phase. H_2S was found to be unstable in a carbonaceous atmosphere at 860 °C and will decompose with the formation of mainly COS and, under increasing oxygen partial pressures, of minor amounts of SO_2 (see Table S1). As the kinetics of this decomposition can hardly be estimated considering the temperature gradients during heating up the gas in the test bench and the catalytic activity of the different materials (Al_2O_3 gas lines, Ni contact mesh, Ni/GDC electrode), the resulting composition in the electrode is unclear. This has to be considered when interpreting the results.

Recordings of resistance contributions from all EIS measurements, including stabilization steps of cell #2, are also given in the ESI in Figure S3. A detailed list of all tested conditions can be found in Table 1. A brief overview of the results, which were not included in the main text of this paper, such as results recorded in fuel cell mode, can be found in the ESI in Figure S4.

3. Results and discussion

Firstly, we show experimental results that evaluate the influence of operating conditions in $H_2O/H_2/N_2$ mixtures (steam to hydrogen ratio, p_{H_2}, p_{H_2O}, current) on the sulfur poisoning behavior of a Ni/GDC electrode, generated with cell #1. Further, we show results derived from $CO_2/CO/N_2$ mixtures, generated with cell #2, where differences between the poisoning behaviors of both atmospheres are pointed out.

3.1. Influence of steam to hydrogen ratio under open circuit conditions

The impact of the steam to hydrogen ratio, which represents conditions along the gas channel in a cell or stack operated at technically meaningful gas conversion rates, is displayed in Fig. 2 for open circuit

Table 1
Overview of the tested gas compositions, current densities and H_2S concentrations.

Cell#	Gas phase / atm	Current densities / Acm^{-2}	H_2S concentrations / ppm
#1	**$H_2O/H_2/N_2$**		
	0.03/0.92/0.05	0, 0.2, 0.5, 0.8	0, 0.1, 0.3, 0.5, 1
	0.475/0.475/0.05	−0.5, 0, 0.5	0, 0.1, 0.3, 0.5, 1
	0.8/0.15/0.05	−1, −0.8, −0.5, −0.2, 0	0, 0.1, 0.3, 0.5, 1
	0.8/0.1/0.1	−1, −0.8, −0.5, −0.2, 0	0, 0.1, 0.3, 0.5, 1
	0.8/0.05/0.15	−1, −0.8, −0.5, −0.2, 0	0, 0.1, 0.3, 0.5, 1
	0.7/0.15/0.15	−0.8, −0.5, −0.2, 0	0, 0.1, 0.3, 0.5, 1
	0.5/0.15/0.35	−0.8, −0.5, −0.2, 0	0, 0.1, 0.3, 0.5, 1
#2	**$CO_2/CO/N_2$**		
	0.8/0.15/0.05	−1[a], −0.8, −0.5, −0.2, 0	≈ 0, 1
	0.8/0.1/0.1	−1[a], −0.8, −0.5, −0.2, 0	≈ 0, 1
	0.8/0.05/0.15	−1[a], −0.8, −0.5, −0.2, 0	≈ 0, 1

[a] 1 Acm^{-2} was only reached under ≈ 0 ppm H_2S, as the cell voltage was limited to a maximum of 1.5 V.

conditions. In Fig. 2a) the measured polarization resistances are shown. For all H_2S concentrations including the H_2S-free gas mixture, the lowest polarization resistance is observed at 0.475 atm steam (steam to hydrogen ratio of 1). Moreover, at all steam concentrations a similar qualitative poisoning behavior can be observed. The initial poisoning step of 0.1 ppm H_2S triggers the highest ASR_{Pol} step size, followed by a smaller continuous increase. Only at a steam to hydrogen ratio of 0.03, the resistance did not further increase after exposure to 0.5 ppm H_2S.

To normalize the poisoning response to the polarization resistance before adding H_2S, the impact of sulfur on the resistance is quantified by the relative increase of the polarization resistance $\Delta ASR_{Pol,rel}$ due to addition of a certain H_2S concentration (x_{H_2S}) and at a partial pressure of steam and/or hydrogen (p_i):

$$\Delta ASR_{Pol,rel}(x_{H_2S}, p_i) = \frac{ASR_{Pol}(x_{H_2S}, p_i) - ASR_{Pol}(0\ \text{ppm}, p_i)}{ASR_{Pol}(0\ \text{ppm}, p_i)} \quad [3]$$

Fig. 2b) shows the relative resistance increase plotted over the steam content. As the impact of sulfur is the highest at steam to hydrogen = 5.33 and lowest at steam to hydrogen = 0.03, an increase in sulfur sensitivity at high steam- and/or low hydrogen concentration can be identified. The steepening slope of the dependence on steam (or hydrogen) partial pressure, which appears within higher H_2S concentrations, demonstrates this sensitivity increase.

A possible cause of this trend could be rooted in the rise of sulfur coverage due to lower H_2 partial pressures [7,40]. To investigate this idea, the $\Delta ASR_{Pol,rel}$ are plotted over the nickel coverage (Θ_S) in Fig. 2c), which is obtained from equation [2]. Generally, the data shows the well-known trend that towards higher nickel coverage a larger impact on the resistance can be expected. However, the measurement points do not exactly follow this trend and a linear fit only yields a rather poor correlation. ($R^2 = 0.813$).

Noteworthy, the points recorded at a steam to hydrogen ratio of 5.33 (denoted with the symbol + in Fig. 2) lie mostly below the trendline. E.g. at a nickel coverage of around 66 % (denoted with a black arrow) the lowest $\Delta ASR_{Pol,rel}$ was measured compared to the other ratios. Therefore, the nickel coverage alone cannot fully explain the observed dependency of the poisoning response on the steam to hydrogen ratio.

3.2. *Influence of p_{H_2} and p_{H_2O} under open circuit conditions*

For the purpose of isolating the influence of hydrogen and steam partial pressures, two variations were performed under H_2S concentrations from 0 to 1 ppm. The hydrogen partial pressure variation was performed from 0.15 atm to 0.05 atm under a constant p_{H_2O} of 0.8 atm (balanced in nitrogen). The high steam content offers a good transferability to practical steam electrolysis inlet conditions. The second variation is introduced later in the text.

The $\Delta ASR_{Pol,rel}$ is plotted over p_{H_2} in Fig. 3a). The data shows a similar trend as the p_{H_2} vs. p_{H_2O} variation, as at low p_{H_2} a stronger response of the resistance to the same H_2S concentration is found. Also, we see that the sensitivity to H_2S at a given p_{H_2}, quantified by the slope of the p_{H_2}-dependency, increases in relation with the H_2S concentration.

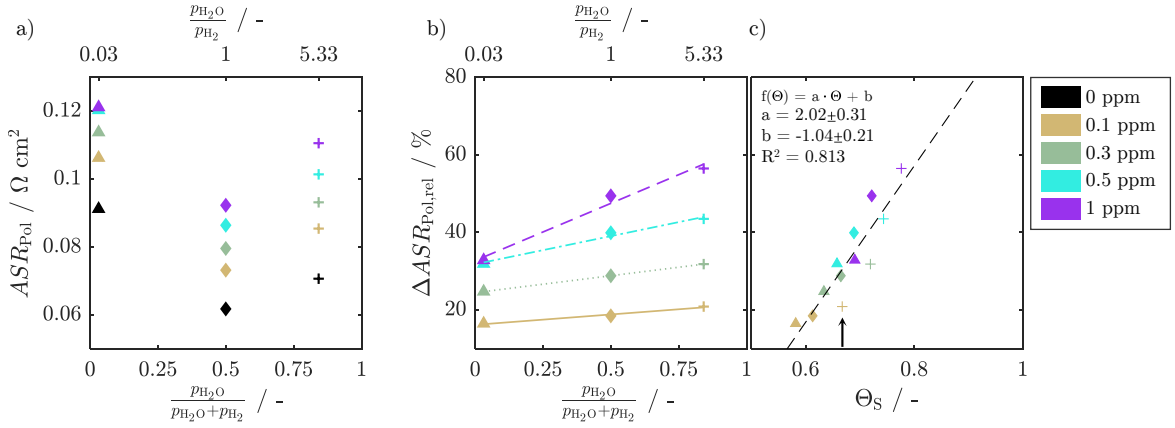

Fig. 2. a) Measured polarization resistances and **b)** calculated relative resistance increase under varying steam and H_2S concentrations balanced in hydrogen and 0.05 atm N_2. Linear fits are added to emphasize the change in concentration dependency. **c)** Data from b) plotted over the theoretical sulfur coverage. The linear fit results in a poor correlation ($R^2 = 0.813$, values behind the fit values denote the standard error). T = 860 °C, OCV.

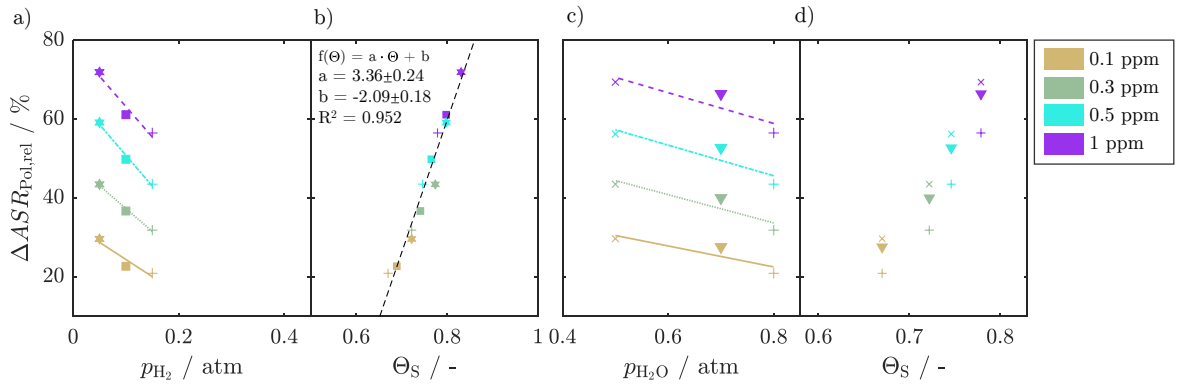

Fig. 3. a) Calculated relative resistance increase under varying hydrogen and H_2S concentrations balanced in nitrogen and 0.8 atm H_2O. **b)** Data from a) plotted over the theoretical sulfur coverage. The linear fit results in a good correlation ($R^2 = 0.952$, values behind the fit values denote the standard error). Hydrogen dependency of poisoning behavior can therefore be attributed to the sulfur coverage **c)** Calculated relative resistance increase under varying steam and H_2S concentrations balanced in nitrogen and 0.15 atm H_2. **d)** Data from c) plotted over the theoretical sulfur coverage. A dependency of poisoning behavior on H_2O concentration cannot be directly attributed to the sulfur coverage on nickel, as the coverage is not influenced by H_2O concentration. $T = 860$ °C, OCV.

However, when the $\Delta ASR_{Pol,rel}$ is now plotted over the nickel coverage, as seen in Fig. 3b), a much clearer correlation can be observed compared to the p_{H_2} vs. p_{H_2O} variation, presented earlier. A linear fit yields an R^2-value of 0.952 showing that the increased sensitivity to H_2S at lower hydrogen concentrations originates from the higher nickel coverage. Qualitatively similar results were earlier reported by Lohsoontorn et al. on symmetrical cells with Ni/GDC electrodes and were also attributed to nickel-sulfur interaction [10]. To demonstrate that the correlation holds across a broader temperature range, the experiment was repeated at 800 °C in a follow-up validation test. The results, shown in Figure S5 (ESI), again revealed a strong correlation between $\Delta ASR_{Pol,rel}$ and nickel coverage ($R^2 = 0.962$).

The second variation was performed at a constant p_{H_2} of 0.15 atm while changing the p_{H_2O} from 0.8 atm to 0.7 atm and 0.5 atm. The resulting $\Delta ASR_{Pol,rel}$ values are displayed in Fig. 3c). The results show that at a low p_{H_2O} the resistance is more sensitive to H_2S addition. Yet, the sensitivity is visibly weaker than at low p_{H_2}. Moreover, the p_{H_2O}-dependency does not seem to change with H_2S concentration, as can be observed from its constant slope. As shown in Fig. 3d), the nickel coverage does not depend on steam partial pressure. A lower p_{H_2O} only results in a vertical shift of $\Delta ASR_{Pol,rel}$. Thus, this newly observed harming effect of low p_{H_2O} can explain why a steam to hydrogen ratio

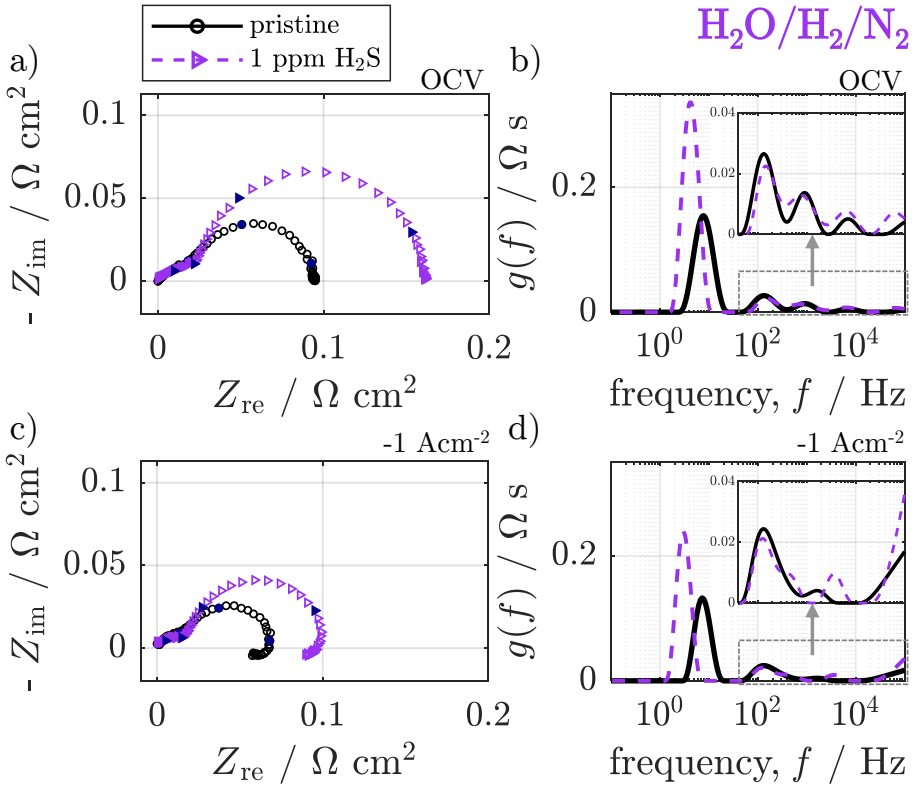

Fig. 4. a) Impedance spectrum and **b)** calculated DRT with 0 ppm and 1 ppm H_2S in OCV. **c)** Impedance spectrum and **d)** calculated DRT with 0 ppm and 1 ppm H_2S under -1 Acm^{-2}. Spectra were recorded with a 0.8 atm H_2O, 0.05 atm H_2, bal. N_2 atmosphere. Blue filled symbols in a) and c) mark points nearest to the decades between 1 Hz and 1 kHz. Ohmic resistances have been removed to highlight changes in polarization resistance contributions. $T = 860$ °C. (For interpretation of the references to color in this figure legend, the reader is referred to the Web version of this article.)

variation only correlates weakly to the nickel coverage (Fig. 2c). In the following, possible reasons for this newly observed effect are discussed.

A reason for this behavior could be that adsorption/dissociation of steam competes for free nickel sites with the equilibrium from equation [2]. However, Rostrup-Nielsen showed experimentally that an influence of steam partial pressure on the nickel-coverage can be excluded [40], which mainly leaves the doped ceria surface as the possible source of the observed behavior. Therefore, we think that either the ceria surface is more likely to interact with H_2S at a higher steam to hydrogen ratio (i.e. a higher p_{O_2}) causing blockage of double-phase-boundaries (DPBs), or the increased p_{O_2} is causing a less active DPB, so that a compensation of lost TPBs by DPBs is less effective. Given that earlier publications suggest that rather a low p_{O_2} than a high p_{O_2} increases H_2S-ceria interactions [10,42,43], the latter option might be more likely. Yet, the doped ceria-H_2S interaction, especially the blocking of active ceria sites via H_2S adsorption, at low H_2S concentrations is rather unexplored. At this point, the previously given explanations for the H_2O concentration dependency are of speculative nature

3.3. Poisoning effects in steam electrolysis mode

As a next step, we evaluate the results generated under cathodic current in the electrolyzer mode and aim to compare it to the observations under OCV. For the here presented analysis, we have selected a gas composition of $p_{H_2}/p_{H_2O}/p_{N_2} = 0.05/0.8/0.15$ atm. At this composition the resistance was most sensitive to H_2S poisoning, as presented in chapter 3.2, and is thus considered to be most suitable to observe differences due to the application of electrolysis load. A direct comparison of the impedance spectra and DRTs between OCV and -1 Acm^{-2}, recorded from the pristine cell and with 1 ppm H_2S is given in Fig. 4. The qualitative change of impedance spectra due to poisoning is similar under load and OCV. Also, it matches earlier reports, as only low frequency contributions are increasing in resistance. These contributions are mainly associated with the Ni/GDC surface chemistry, as well as concentration losses [12,32,41,44]. When we compare the spectra under OCV and load, we see that the electrode gets visibly activated due to the load application. Interestingly, the activation is more strongly expressed when the electrode is in the poisoned state, ultimately resulting in a lower resistance difference between poisoned and pristine.

Low-frequency inductive contributions (i.e. a single inductive hook) started to appear when a current density of $|j| > 0.5$ Acm^{-2} was applied, exemplarily shown in Fig. 4c) for -1 Acm^{-2}. The size and shape of the hook was mainly determined by the absolute value of the applied current, thus it appeared in fuel cell as well as in electrolyzer mode. Furthermore, no relation to the gas composition nor to the H_2S concentration was found. Measurement artefacts due to nonlinearities or instationarities were excluded by analyzing the Kramers-Kronig residuals, confirming the validity of the spectra. In literature, a variety of phenomena are discussed from which such hooks could arise. Explanations include a two-step reaction which involves an intermediate [45,46], a relation to the deposition of Si impurities [47], or the reduction of the zirconia electrolyte due to a too high overpotential [48]. The origin of the inductive hook observed in these measurements is not yet known and will be addressed in future studies. However, since no relation to the H_2S concentration was found, inductive contributions were neglected in the present analysis.

To get a clearer picture, the calculated $\Delta ASR_{Pol,rel}$ values as a function of electrolysis load, up to -1 Acm^{-2} are given in Fig. 5a). A clear trend is observable: $\Delta ASR_{Pol,rel}$ decreases with current density. Also, the effect is magnified when the H_2S concentration is increased. Multiple authors have observed a similar effect when polarizing a poisoned solid oxide fuel cell [8,9,12,14]. To the best of our knowledge, this is the first time a mitigation of the H_2S-induced resistance increase was observed as a direct consequence of the application of electrolysis load.

Fig. 5b) displays the $\Delta ASR_{Pol,rel}$ as a function of Θ_S calculated from the inlet concentrations. For the sake of clarity, only the values recorded under OCV (stars) as well as under -1 Acm^{-2} electrolysis load (circles) are plotted. The OCV trendline, previously obtained in Fig. 3b) is additionally shown as a reference. The maximum mitigation of the resistance increase under identical theoretical coverage corresponds to a 37 % improvement under load compared to OCV, as signified by the grey arrows.

Possibly, the local evolution of hydrogen could increase the hydrogen concentration close to the nickel surface which would effectively reverse reaction [1]. To correct the effect of the locally increased hydrogen concentration we have performed a p_{H_2}-correction according to the following equation, based on Fick's law [33,49]:

$$p_{H_2}^{TPB/DPB} = p_{H_2}^{channel} - \frac{1}{G_{eff}} \frac{\widetilde{R}T}{2FD_{H_2}^{mol}} j \cdot \left(1.0133 \cdot 10^5 \frac{Pa}{atm}\right)^{-1} \quad [4]$$

with $\widetilde{R}$ denoting the gas constant, T the temperature, F the Faraday constant, $D_{H_2}^{mol}$ the molar diffusion coefficient of hydrogen and j the current density. G_{eff} stands for the geometry parameter, which includes effective microstructural properties, as well as the diffusion length. We have used a G_{eff} value of 744 m^{-1}, as derived in Ref. [33] for the same testbench- and cell-type. For more information on the derivation and usage of the microstructure parameter we forward the reader to our earlier publications [32,33,50]

From the p_{H_2}-correction one can calculate a local coverage, which is

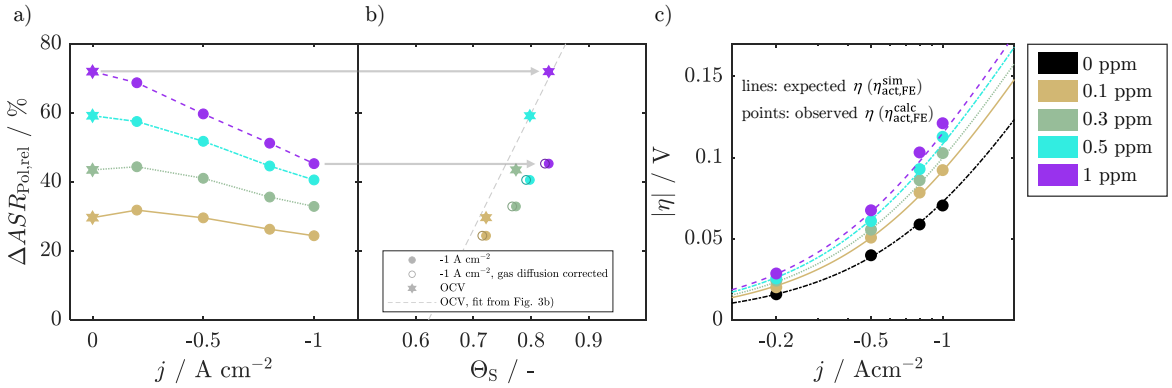

Fig. 5. a) Calculated relative resistance increase under varying cathodic load of the Ni/GDC electrode and H_2S concentrations recorded in a 0.8 atm H_2O, 0.05 atm H_2, bal. N_2 atmosphere. **b)** Selected data from a) plotted over the theoretical sulfur coverage according to concentrations in the gas channel and estimated at the reaction zone. **c)** Observed and expected electrode overpotential at identical conditions from a). While relative resistance increase shows a down-trend with higher cathodic load, the overpotential matches estimation from a parametrized Butler-Volmer equation. The behavior in a) can therefore be attributed to the inherent Tafel behavior of the electrochemical reaction. $T = 860$ °C.

only marginally lower than the one calculated from the channel conditions, as also displayed in Fig. 5b). Thus, a local excess of hydrogen cannot be a suitable explanation for the observed mitigation of the resistance increase. Significant concentration differences due to gas conversion can also be ruled out, as the total conversion at -1 Acm^{-2} and 0.16 nL min^{-1} steam is approximately 4.4 %.

Multiple authors suggest that electrode activation, i.e. the inherent Tafel behavior of the electrochemical reaction, could explain the mitigation of resistance increase observed on solid oxide fuel cells [17–19]. A similar influence can be expected under electrolysis load. To test this hypothesis, we have calculated the electrode overpotential from our measurement data using an "OCV minus losses" model [33,49,51].

$$U_{cell} = U_{OCV} - \eta_{ohm} - \eta_{act,FE} - \eta_{Diff,FE} - \eta_{act,AE} - \eta_{Diff,FE} \quad [5]$$

Maximum expectable values of the overpotentials resulting from the air electrode due to gas diffusion $\eta_{Diff,AE}$ and activation losses $\eta_{act,AE}$ were estimated to be -1.7 mV and -0.35 mV, respectively, at -1 Acm^{-2} [33,51]. Therefore, their contributions can be neglected under the presented conditions. The overpotential from activation of the fuel electrode $\eta^{calc}_{act,FE}$ can then be easily observed from calculating:

$$\eta^{calc}_{act,FE} = -U_{cell} + U_{OCV} - \eta_{Diff,FE} - \eta_{ohm} \quad [6]$$

In this way, no three-electrode setup is needed to extract the fuel electrode overpotential and we can directly calculate the fuel electrode overpotential from measurements in the two-electrode setup. For the calculation of the gas diffusion overpotential we refer again to our earlier publications [33,49,51]. The overpotentials observed at 0 ppm were then used to fit a Butler-Volmer expression to the overpotential values. The fit yielded a charge transfer coefficient α_{FE} of 0.5, which is close to the published value in Ref. [33] for the same electrode. Exchange current densities j_0 were derived from the respective activation resistance $ASR_{act,FE}$ at OCV according to Ref. [49]:

$$j_0 = \frac{1}{ASR_{act,FE}} \cdot \frac{\tilde{R}T}{2F} \quad [7]$$

As seen in Fig. 5c), the method yields an excellent fit to the data when no H_2S is added. Now we assume that the addition of H_2S only decreases the exchange current density. Thus, we calculate the exchange current densities from the resistances after H_2S poisoning at OCV assuming that charge transfer coefficients stay constant. We can then simulate the expected overpotential $\eta^{sim}_{act,FE}$ as a function of current density and compare it to the calculated overpotential $\eta^{calc}_{act,FE}$. As seen in Fig. 5c), this method yields a very good prediction of the overpotential at all poisoning stages. In other words, the behavior under load matches the overpotential expected by the inherent Tafel behavior of the electrochemical kinetics. Therefore, no mitigation of the poisoning response due to cathodic load application is found and the lowering of $\Delta ASR_{Pol,rel}$ values with higher electrolysis load can be fully explained by a Butler-Volmer type cathodic activation.

3.4. Poisoning effects on operation with carbonaceous gases in OCV

According to various resources, the poisoning behavior under carbonaceous gases can differ significantly from the one observed under a hydrogen-steam atmosphere. Riegraf et al. found a high sensitivity of Ni/GDC electrodes to sulfur contaminations in the 100 ppb range during CO_2 electrolysis [3]. Similar observations were earlier reported by Ebbesen and Mogensen for Ni/YSZ fuel electrode supported electrolysis cells [22]. Previously, it has been speculated that the reason for the higher sensitivity to sulfur under carbonaceous gases is a weaker interaction between CO and adsorbed sulfur, compared to hydrogen and adsorbed sulfur, eventually resulting in higher nickel coverages.

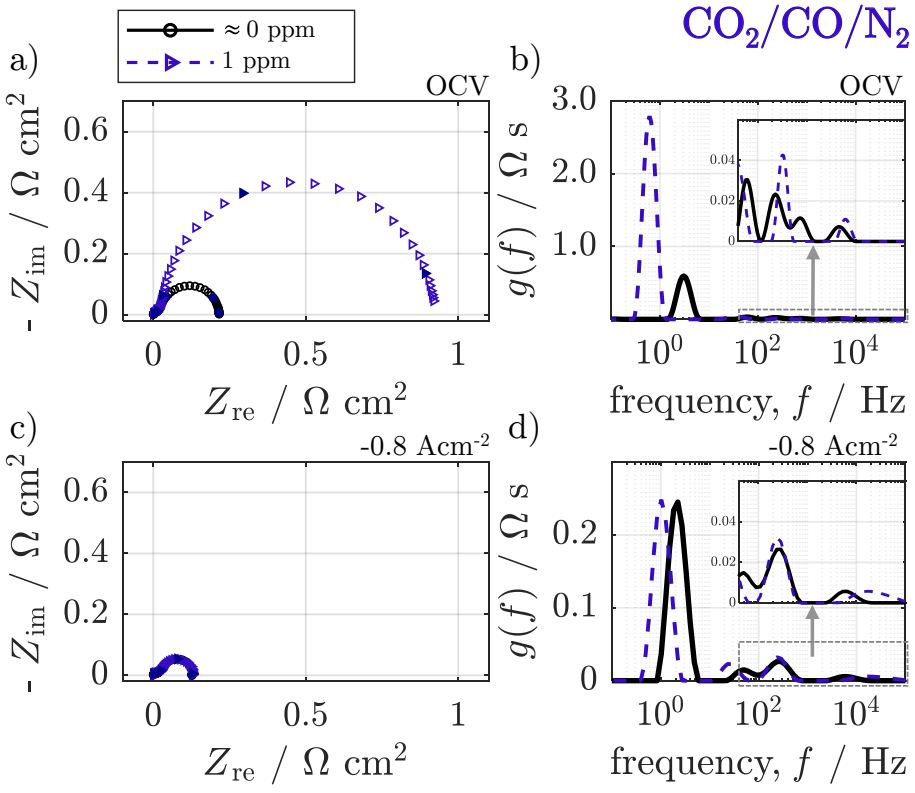

Fig. 6. a) Calculated relative resistance increase under 1 ppm H_2S and varying CO concentrations balanced in nitrogen and 0.8 atm CO_2 in OCV. The values obtained from an equivalent $H_2O/H_2/N_2$ experiment are also displayed in light colors. **b)** Calculated relative resistance increase under varying cathodic load of the Ni/GDC electrode and 0.05 atm CO balanced in nitrogen and 0.8 atm CO_2. The relative resistance increase at -0.8 Acm^{-2} is approximately zero. $T = 860$ °C. (For interpretation of the references to color in this figure legend, the reader is referred to the Web version of this article.)

Carbonaceous feed streams are more likely to be contaminated with sulfur species. Therefore, the previously described measurements were transferred to a CO/CO_2 system with cell #2. Unfortunately, contamination of our feedgas was found to be non-negligible. Low concentrations (sub-100 ppb) of SO were confirmed to be present in the CO_2 feed by mass spectrometry. As reported in Ref. [3], an increase in polarization resistance appeared after the atmosphere was switched from pure hydrogen to CO/CO_2 while trying to record a first "pristine" dataset, complicating a stable recording of data. More precisely, when the protocol was started with a 0.8 atm/0.15 atm/0.05 atm $CO_2/CO/N_2$ mixture, a polarization resistance of 127 $m\Omega cm^2$ was measured at OCV, which was found to have increased to 160 $m\Omega cm^2$, 9 h after the protocol started. This increase was perfectly reversible after switching the atmosphere back to 100 % H_2 for 5 h.

However, after letting the cell stabilize for 24 h in a 0.8 atm/0.15 atm/0.05 atm $CO_2/CO/N_2$ mixture under OCV, the polarization resistance reached a stable point and a second dataset was recorded. Thereby, polarization resistances at the respective concentrations remained stable before and after the protocol.

Afterwards, the H_2S concentration was increased by 1 ppm. The cell impedance was then again stabilized for 24 h and a third dataset was recorded. $\Delta ASR_{Pol,rel}$ values presented in the following are calculated from the differences between the second and third dataset. In this way, the "reference state" (second dataset) is not completely sulfur free. However, the resistance increase observed between the second and third dataset was significantly larger than the one observed between the first and second dataset. To further confirm the stability of the established baseline state, a reference experiment was conducted in which the resistance was continuously monitored for 70 h in a 0.8 atm CO_2/0.2 atm CO atmosphere at 860 °C (without external sulfur addition) after switching from a steam/hydrogen atmosphere. The experiment demonstrated an increase of resistance (caused by intrinsic sulfur impurities of the CO_2/CO feed) within a 20 h stabilization period, followed by a 50 h long stable plateau. (Figure S6, ESI).

To firstly understand concentration effects on the poisoning behavior under CO_2-electrolysis, we analyze the sensitivity of the resistance to H_2S addition at different CO partial pressures under OCV conditions. Three CO partial pressures have been tested, namely 0.15 atm, 0.1 atm, 0.05 atm in constant 0.8 atm CO_2 and balanced in nitrogen. We recorded the impedance with and without the addition of 1 ppm H_2S. The resulting $\Delta ASR_{Pol,rel}$ values evaluated over p_{CO} are displayed in Fig. 6a). The values earlier obtained from $H_2O/H_2/N_2$ are also displayed as a comparison. Interestingly, the poisoning response to 1 ppm H_2S in a $CO_2/CO/N_2$ mixture is significantly stronger than the one observed earlier in the $H_2O/H_2/N_2$ mixture. More precisely, under the lowest tested CO partial pressure, the impact of sulfur on the resistance is nearly 5 times larger compared to the equivalent $H_2O/H_2/N_2$ mixture.

Also, we see that the CO concentration dependency is much more strongly expressed than the earlier observed equivalent hydrogen concentration dependency. The resistance is therefore around 1.5 times more sensitive to H_2S poisoning at 0.05 atm CO than at 0.15 atm CO. The strong dependency on CO partial pressure indicates a key role of CO in removing adsorbed sulfur from the nickel surface in carbonaceous atmospheres.

3.5. Poisoning effects on CO_2 electrolysis

Further, the gas mixtures have also been tested under electrolysis load. Again, we focus on the point which is most sensitive to H_2S poisoning, i.e. 0.05 atm CO. Fig. 6b) shows the $\Delta ASR_{Pol,rel}$ values plotted over the electrolysis load applied. Despite the detrimental effect of H_2S at OCV, a very strong mitigation of the resistance increase was found with the application of electrolysis load. Most remarkably, at −0.8 Acm^{-2} polarization resistance values were identical with and without the addition of H_2S. The actual measured impedance spectra and calculated DRTs are displayed in Fig. 7. At OCV the increase in

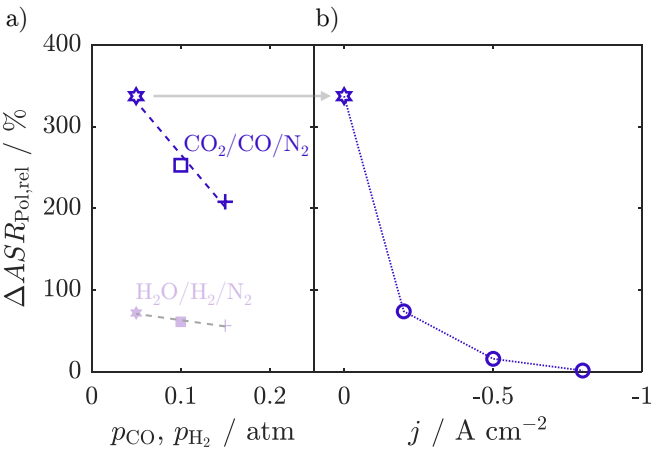

Fig. 7. **a)** Impedance spectra and **b)** calculated DRT with 0 ppm and 1 ppm H_2S in OCV. **c)** Impedance spectra and **d)** calculated DRT with 0 ppm and 1 ppm H_2S under −0.8 Acm^{-2}. Spectra were recorded with a 0.8 atm CO_2, 0.05 atm CO, bal. N_2 atmosphere. Scale in d) is adjusted for visibility. Blue filled symbols in a) and c) mark points nearest to the decades between 0.1 Hz and 1 kHz. Ohmic resistances have been removed to highlight changes in polarization resistance contributions. T = 860 °C. (For interpretation of the references to color in this figure legend, the reader is referred to the Web version of this article.)

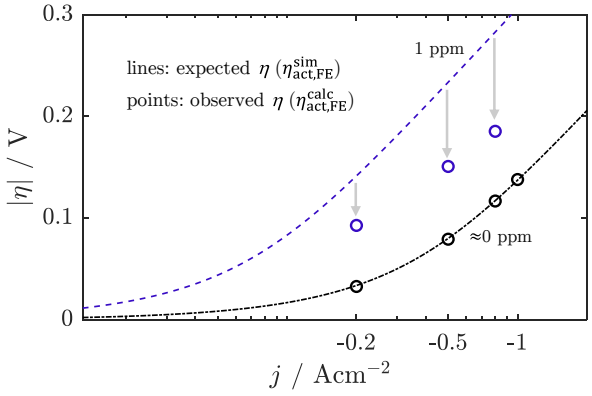

Fig. 8. Observed and expected electrode overpotential under varying cathodic load of the Ni/GDC electrode and 0.05 atm CO balanced in nitrogen and 0.8 atm CO_2 with 0 and 1 ppm H_2S added. When no H_2S is added, the electrode overpotential can be well described by a parametrized Butler-Volmer equation, while at 1 ppm the electrode overpotential is significantly lower than it would be expectable by the inherent Tafel behavior. T = 860 °C.

polarization resistance is found in the low frequency contribution, qualitatively similar to the poisoning response under $H_2O/H_2/N_2$ atmospheres, but significantly larger. Low-frequency inductive contributions were also found to be present in an identical manner as under $H_2O/H_2/N_2$.

Impedance spectra recorded under −0.8 Acm^{-2} electrolysis load, with and without H_2S addition, are indistinguishable in the Nyquist representation. The DRTs show a slight difference in the peak frequency of the low frequency contribution, indicating a higher chemical capacitance, which may be caused by stronger reduction of the ceria due to an increased negative overpotential.

As discussed earlier in the text, the relative resistance increase is not the most suitable measure for resolving the poisoning behavior under load. Therefore, we have also calculated the overpotential $\eta^{calc}_{act,FE}$ at the fuel electrode with the same method as described earlier, which is displayed in Fig. 8. We see that, despite the fact that polarization

resistances were close to the pristine state, a significant increase in overpotential is observable at all current loads. This is due to the fact that the resistance value originates from the slope of a $j-\eta$ curve ($ASR_{FE} = \frac{d\eta}{dj}$), so that the same resistance can be observed at different overpotentials when their slopes over j are identical.

However, we can use the same strategy as described in 3.3 to calculate an exchange current density, fit the charge transfer coefficient $\alpha_{FE}^{CO_2}$ at ≈ 0 ppm and simulate the expected overpotential $\eta_{act,FE}^{sim}$. The fit for $\alpha_{FE}^{CO_2}$ resulted in a value of 0.46 and can perfectly represent the overpotential at ≈ 0 ppm up to -1 Acm^{-2}.

Thereby, under an added concentration of 1 ppm H_2S, a measured overpotential of around 100 mV lower than the expected one can be observed. This shows that there is a definite poisoning mitigation effect due to cathodic current under CO_2 electrolysis, contrary to steam electrolysis.

While the exact reason for the observed mitigation effect under sulfur-poisoned CO_2-electrolysis is unclear at this stage, the following discussion based on previous literature findings on the electrochemical conversion of CO_2 on doped ceria aims to offer a possible explanation for the observed behavior. Riegraf et al. suggested that the CO oxidation mechanism on GDC proceeds to a higher fraction on the GDC|gas double-phase-boundary, compared to H_2 oxidation [35]. Similar effects could be expected when the electrode is set under cathodic polarization. Moreover, it is known that adsorbate-adsorbate interactions facilitate CO_2 reduction when a doped ceria surface is more cathodically polarized [52]. Equivalent effects were not found under H_2/H_2O mixtures [52,53]. Thus, we speculate that a poisoning-induced increase in electron consumption through the DPB pathway that results in a more activated doped ceria surface could ultimately cause a lower overpotential than one would expect from the inherent Tafel behavior. However, proving this speculation would require more fundamental investigations, which are beyond the scope of this work.

4. Conclusions

We investigated the H_2S-induced poisoning behavior of a Ni/GDC electrode by means of electrochemical impedance spectroscopy and electrode overpotential under cathodic polarization. Both H_2O and CO_2 electrolysis were investigated to assess their sensitivity to sulfur poisoning.

For the OCV conditions in $H_2O/H_2/N_2$ environments, a strong dependence of the poisoning response on H_2 partial pressure was shown, which can be well correlated with sulfur adsorption on the nickel surface, described by a Temkin-isotherm. Also, the relative resistance increase showed a lower but non-negligible dependency on H_2O partial pressure, which cannot be attributed to sulfur adsorption on the nickel surface.

Under cathodic polarization, the relative resistance increase was found to decrease at higher current densities. However, the electrode overpotential matched expectations from the inherent Tafel behavior, which explains the apparent change in the resistance response. Therefore, we conclude that cathodic load does not mitigate the H_2S poisoning in $H_2O/H_2/N_2$ mode.

In $CO_2/CO/N_2$ environments, when no external current is applied, the cell exhibited a greater sensitivity to poisoning. Particularly, the poisoning response changed more strongly when the CO concentration was lowered, than due to an equivalent lowering of H_2 concentration in a $H_2O/H_2/N_2$ atmosphere.

In contrast, the polarization resistance appeared unchanged between poisoned and unpoisoned conditions when a current of -0.8 Acm^{-2} was applied to the carbonaceous system, but the electrode overpotential was notably larger. However, this increase in overpotential was still significantly lower than predicted by the inherent Tafel behavior, highlighting a clear mitigation effect of cathodic current in CO_2-electrolysis.

CRediT authorship contribution statement

D. Esau: Writing – original draft, Methodology, Investigation, Formal analysis, Data curation, Conceptualization. **S.A. Horlick:** Writing – review & editing, Resources, Conceptualization. **C.-Y. Tsai:** Writing – review & editing, Resources, Conceptualization. **A. Weber:** Writing – review & editing, Supervision, Project administration, Methodology, Investigation, Funding acquisition, Conceptualization.

Declaration of generative AI and AI-assisted technologies in the writing process

During the preparation of this work the authors used ChatGPT in order to improve readability and grammar of the manuscript. After using this tool, the authors reviewed and edited the content as needed and take full responsibility for the content of the published article.

Declaration of competing interest

The authors declare that they have no known competing financial interests or personal relationships that could have appeared to influence the work reported in this paper.

Acknowledgments

The authors gratefully acknowledge funding from the Federal Ministry of Research, Technology and Space in the project H2Giga-HTEL-Stacks (BMBF 03HY124C). Sincere thanks are given to *Sunfire SE* and *Kerafol GmbH & Co. KG* for producing the test cells.

Appendix A. Supplementary data

Supplementary data to this article can be found online at https://doi.org/10.1016/j.jpowsour.2025.238429.

Nomenclature

latin letters	
$ASR/\Delta ASR_{Pol,rel}$	Area specific resistance (Ωcm^2)/relative increase in polarization resistance (-)
D_i^{mol}	Molar diffusion coefficient (cm^2 s^{-1})
F	Faraday constant 96485 (C mol^{-1})
G_{eff}	Effective geometry parameter (m^{-1})
j	Current density (Acm^{-2})
j_0	Exchange current density (Acm^{-2})
p_i	Partial pressure of component i (atm)
$\tilde{R}$	Specific gas constant 8.314 (J mol^{-1} K^{-1})

(*continued on next page*)

(*continued*)

T	Temperature (°C)
x_{H_2S}	Molar fraction of H_2S (ppm)

greek letters

α	Charge transfer coefficient (-)
γ	Exponential pre-factor (A m^{-2})
η_i	Overpotential contribution from process i (V)
Θ	Coverage (-)

Sub- and superscripts

cell	Cell
act	Activation
AE	Air electrode
calc	Calculated (observed)
Diff	Diffusion
FE	Fuel electrode
Ohm	Ohmic
Pol	Polarization
rel	Relative
sim	Simulated (expected)

abbreviations

GDC	Gadolinium-Doped Ceria
CO	Carbon monoxide
CO_2	Carbon dioxide
COS	Carbonyl sulfide
DRT	Distribution of relaxation times
EIS	Electrochemical impedance spectroscopy
ESI	Electronic supporting information
H_2	Hydrogen
H_2S	Hydrogen sulfide
LSCF	Lanthanum strontium cobalt iron oxide
N_2	Nitrogen
Ni	Nickel
OCV	Open-circuit voltage
R-CPE	Resistance parallel to a constant phase element
S	Sulfur
SOE(C)	Solid Oxide Electrolyzer (Cell)
SOx	Sulfur oxide species
YSZ	Yttria-stabilized zirconia

Data availability

Data can be found under the DOI: https://doi.org/10.35097/ze6dcjvbp419wvc4.

References

[1] A. Hauch, R. Küngas, P. Blennow, A.B. Hansen, J.B. Hansen, B.V. Mathiesen, M. B. Mogensen, Science 370 (2020) eaba6118.
[2] M. Mueller, M. Klinsmann, U. Sauter, J.-C. Njodzefon, A. Weber, Chem. Ing. Tech. 96 (2024) 143–166.
[3] M. Riegraf, K. Develos-Bagarinao, I. Biswas, R. Costa, J. Power Sources 559 (2023) 232669.
[4] R.T. Porter, M. Fairweather, M. Pourkashanian, R.M. Woolley, Int. J. Greenh. Gas Control 36 (2015) 161–174.
[5] T. Feng, M. Huo, X. Zhao, T. Wang, X. Xia, C. Ma, Chem. Eng. Res. Des. 121 (2017) 191–199.
[6] T. Feng, X. Zhao, T. Wang, X. Xia, M. Zhang, Q. Huan, C. Ma, Energy Fuels 30 (2016) 6578–6584.
[7] I. Alstrup, J.R. Rostrup-Nielsen, S. Røen, Appl. Catal. 1 (1981) 303–314.
[8] J.B. Hansen, Electrochem. Solid State Lett. 11 (2008) B178.
[9] Z. Cheng, S. Zha, M. Liu, J. Power Sources 172 (2007) 688–693.
[10] P. Lohsoontorn, D. Brett, N. Brandon, J. Power Sources 183 (2008) 232–239.
[11] J. Nielsen, B.R. Sudireddy, A. Hagen, Å.H. Persson, J. Electrochem. Soc. 163 (2016) F574.
[12] M. Riegraf, V. Yurkiv, R. Costa, G. Schiller, K.A. Friedrich, ChemSusChem 10 (2017) 587–599.
[13] S.K. Schubert, M. Kusnezoff, A. Michaelis, S.I. Bredikhin, J. Power Sources 217 (2012) 364–372.
[14] E. Brightman, D.G. Ivey, D.J. Brett, N.P. Brandon, J. Power Sources 196 (2011) 7182–7187.
[15] A. Hagen, G.B. Johnson, P. Hjalmarsson, J. Power Sources 272 (2014) 776–785.
[16] S. Zha, Z. Cheng, M. Liu, J. Electrochem. Soc. 154 (2006) B201.
[17] Z. Cheng, J.-H. Wang, Y. Choi, L. Yang, M.-C. Lin, M. Liu, Energy Environ. Sci. 4 (2011) 4380–4409.
[18] V.M. Janardhanan, D.S. Monder, J. Electrochem. Soc. 161 (2014) F1427.
[19] M. Riegraf, G. Schiller, R. Costa, K.A. Friedrich, A. Latz, V. Yurkiv, J. Electrochem. Soc. 162 (2014) F65.
[20] G. Jeanmonod, S. Diethelm, J. Van Herle, J. Phys.: Energy 2 (2020) 034002.
[21] T.L. Skafte, P. Blennow, J. Hjelm, C. Graves, J. Power Sources 373 (2018) 54–60.
[22] S.D. Ebbesen, M. Mogensen, J. Power Sources 193 (2009) 349–358.
[23] K.K.F.G.C. Kg, in, Kerafol® Keramische Folien Gmbh & Co. KG, Eschenbach, Germany..
[24] R.T. Leah, A. Bone, E. Hammer, A. Selcuk, M. Rahman, A. Clare, S. Mukerjee, M. Selby, ECS Trans. 78 (2017) 87.
[25] J. Aicart, L. Tallobre, A. Surrey, B. Gervasoni, C. Geipel, H. Fontaine, S. Desousanobre, J. Mougin, Int. J. Hydrogen Energy 60 (2024) 531–539.
[26] I.D. Unachukwu, V. Vibhu, I.C. Vinke, R.-A. Eichel, L.B. de Haart, J. Power Sources 556 (2023) 232436.
[27] I.D. Unachukwu, V. Vibhu, J. Uecker, I.C. Vinke, R.-A. Eichel, L.B. de Haart, J. CO2 Util. 69 (2023) 102423.
[28] A. Nenning, C. Bischof, J. Fleig, M. Bram, A.K. Opitz, Energies 13 (2020) 987.
[29] C. Grosselindemann, F. Kullmann, T. Lehnert, O. Fritz, F.M. Fuchs, A. Weber, Fuel Cells 23 (2023) 442–453.
[30] P. Kim-Lohsoontorn, J. Bae, J. Power Sources 196 (2011) 7161–7168.
[31] S. Primdahl, Y.-L. Liu, J. Electrochem. Soc. 149 (2002) A1466.

[32] D. Esau, C. Grosselindemann, S. Sckuhr, F. Kullmann, A. Lindner, Z. Liang, F. Fuchs, A. Weber, J. Electrochem. Soc. 171 (2024) 054522.
[33] C. Grosselindemann, N. Russner, S. Dierickx, F. Wankmüller, A. Weber, J. Electrochem. Soc. 168 (2021) 124506.
[34] A. Weber, S. Dierickx, N. Russner, E. Ivers-Tiffée, ECS Trans. 77 (2017) 141.
[35] M. Riegraf, M.P. Hoerlein, R.m. Costa, G.n. Schiller, K.A. Friedrich, ACS Catal. 7 (2017) 7760–7771.
[36] D. Klotz, A. Weber, E. Ivers-Tiffée, Electrochim. Acta 227 (2017) 110–126.
[37] M. Schönleber, D. Klotz, E. Ivers-Tiffée, Electrochim. Acta 131 (2014) 20–27.
[38] M. Riegraf, R. Costa, G. Schiller, K.A. Friedrich, S. Dierickx, A. Weber, J. Electrochem. Soc. 166 (2019) F865.
[39] J. Schefold, A. Brisse, M. Zahid, J. Electrochem. Soc. 156 (2009) B897.
[40] J.R. Rostrup-Nielsen, J. Catal. 21 (1971) 171–178.
[41] F. Kullmann, A. Schwiers, M. Juckel, N. Menzler, A. Weber, J. Electrochem. Soc. 171 (2024) 044511.
[42] P. Lohsoontorn, D.J. Brett, N.P. Brandon, J. Power Sources 175 (2008) 60–67.
[43] Y. Zeng, S. Kaytakoglu, D. Harrison, Chem. Eng. Sci. 55 (2000) 4893–4900.
[44] F. Kullmann, D. Esau, K. Limbeck, S. Dierickx, A. Lindner, H. Störmer, A. Weber, J. Power Sources 625 (2025) 235621.
[45] D. Klotz, Electrochem. Commun. 98 (2019) 58–62.
[46] B. Van Hassel, B.A. Boukamp, A. Burggraaf, Solid State Ionics 48 (1991) 139–154.
[47] A. Nechache, B.A. Boukamp, M. Cassir, A. Ringuedé, J. Solid State Electrochem. 23 (2019) 109–123.
[48] K.V. Hansen, M. Chen, T. Jacobsen, K. Thyden, S.B. Simonsen, S. Koch, M. B. Mogensen, J. Electrochem. Soc. 163 (2016) F1217.
[49] A. Leonide, Y. Apel, E. Ivers-Tiffee, ECS Trans. 19 (2009) 81.
[50] D. Ewald, C. Großelindemann, D. Esau, F.-M. Fuchs, A. Weber, J. Electrochem. Soc. 171 (2024) 044506.
[51] J.-C. Njodzefon, D. Klotz, A. Kromp, A. Weber, E. Ivers-Tiffée, J. Electrochem. Soc. 160 (2013) F313.
[52] Z.A. Feng, M.L. Machala, W.C. Chueh, Phys. Chem. Chem. Phys. 17 (2015) 12273–12281.
[53] Z.A. Feng, F. El Gabaly, X. Ye, Z.-X. Shen, W.C. Chueh, Nat. Commun. 5 (2014) 4374.